Atmos. Chem. Phys. Discuss., https://doi.org/10.5194/acp-2018-1246
Manuscript under review for journal Atmos. Chem. Phys.
Discussion started: 10 December 2018
© Author(s) 2018. CC BY 4.0 License.

Atmospheric Chemistry and Physics Discussions

Spatial distribution and temporal trend of ozone pollution in China observed with the OMI satellite instrument, 2005-2017

Lu Shen[1], Daniel J. Jacob[1], Xiong Liu[2], Guanyu Huang[3], Ke Li[1], Hong Liao[4]

[1]John A. Paulson School of Engineering and Applied Sciences, Harvard University, Cambridge, MA 02138, USA
[2]Harvard-Smithsonian Center for Astrophysics, Cambridge, Massachusetts 02138, USA
[3]Environmental & Health Sciences, Spelman College, Atlanta, Georgia 30314, USA
[4]School of Environmental Science and Engineering, Nanjing University of Information Science & Technology, Nanjing 210044, China

Correspondence to: Lu Shen (lshen@fas.harvard.edu)

Abstract. We use data from the new China Ministry of Ecology and Environment (MEE) network to show that OMI satellite observations of tropospheric ozone can successfully map the distribution of surface ozone pollution in China and the frequency of high-ozone episodes. After subtracting the Pacific background, OMI ozone enhancements over China can quantify mean summer afternoon surface ozone with a precision of 10.7 ppb and a spatial correlation coefficient R=0.73. Day-to-day correlations between OMI and the MEE ozone data are statistically significant but limited by noise in the individual OMI retrievals. OMI shows significantly higher values on surface ozone episode days (>82 ppb). An extreme value model can successfully predict the probability of surface ozone episodes from the daily OMI data. The 2005-2017 OMI record shows a 0.67 ppb a^{-1} increase in mean summer afternoon ozone in eastern China and an increasing frequency of ozone pollution episodes particularly in the north.

Atmos. Chem. Phys. Discuss., https://doi.org/10.5194/acp-2018-1246
Manuscript under review for journal Atmos. Chem. Phys.
Discussion started: 10 December 2018
© Author(s) 2018. CC BY 4.0 License.

Atmospheric Chemistry and Physics Discussions

1 Introduction

Ozone in surface air is harmful to public health (Bell et al., 2004). It is produced by photochemical oxidation of volatile organic compounds (VOCs) in the presence of nitrogen oxides ($NO_x \equiv NO + NO_2$). Both VOCs and NO_x are emitted in large amounts in polluted regions by fuel combustion and industry. Ozone pollution is a particularly severe problem in China, where the air quality standard of 82 ppb (maximum 8-h daily average) is frequently exceeded (Wang et al., 2017). Observations in eastern China have reported increasing ozone trends of 1-3 ppb a^{-1} over the past decade (Sun et al., 2016; Gao et al., 2017; Ma et al., 2017; Li et al., 2018). The surface observations were very sparse until 2013, when data from a national network of ~1000 sites operated by the China Ministry of Ecology and Environment (MEE) started to become available. Here we use the MEE network data to demonstrate the ability of the space-based Ozone Monitoring Instrument (OMI) to observe ozone pollution in China, and we use the OMI data going back to 2005 to infer long-term ozone pollution trends.

OMI measures atmospheric ozone absorption by solar backscatter in the UV (270-365 nm) (Levelt et al., 2006). It follows a long lineage of UV satellite instruments (TOMS series starting in 1979, GOME series starting in 1995) directed primarily at monitoring the total ozone column. Retrieval of tropospheric ozone (only ~10% of the column) from these instruments has mostly been done in the past by subtracting independent satellite measurements of stratospheric ozone (Fishman et al., 1987; Ziemke et al., 2011). OMI has sufficiently fine spectral resolution to allow direct retrieval of tropospheric ozone although the sensitivity decreases toward the surface because of Rayleigh scattering (Liu et al., 2010). The direct retrieval typically provides one piece of information for the tropospheric ozone column weighted towards the middle troposphere (Zhang et al., 2010).

A number of previous studies have shown that satellite observations of ozone can detect surface ozone pollution events (Fishman et al., 1987; Shim et al., 2009; Eremenko et al., 2008; Hayashida et al., 2008;), including for Chinese urban plumes (Kar et al., 2010; Hayashida et al., 2015). Even if sensitivity to the lower troposphere is low, the enhancements can be sufficiently large to enable detection. However, no quantitative comparison to surface observations has so far been done. Surface ozone network data are available in the US and Europe but levels are generally too low to enable statistically meaningful validation. The MEE network in China provides a unique opportunity.

2 Data and Methods

We use the OMI Ozone Profile retrieval (PROFOZ v0.9.3, level 2) product (Liu et al., 2010; Kim et al., 2013; Huang et al., 2017, 2018) from the Smithsonian Astrophysical Observatory (SAO). OMI is in polar sun-synchronous orbit with a 1330

© Author(s) 2018. CC BY 4.0 License.

local observation time, and provides daily global mapping with 13×24 km^2 nadir pixel resolution (Levelt et al., 2006). Partial ozone columns are retrieved by PROFOZ for 24 vertical layers, of which 3-7 are in the troposphere with pressure levels dependent on tropopause and surface pressure (Liu et al., 2010). The retrieval uses a Bayesian optimization algorithm with prior information from the McPeters et al. (2007) climatology varying only by latitude and month. Averaging kernel matrices quantifying retrieval sensitivity are provided for individual retrievals. The trace of the averaging kernel matrix below a certain retrieval pressure (degrees of freedom for signal or DOFS) estimates the number of independent pieces of information on ozone profile below that pressure. The DOFS for the tropospheric ozone column in summer as retrieved by PROFOZ is about 1 (Zhang et al., 2010). The PROFOZ tropospheric retrievals have been successfully validated with ozonesonde data (Huang et al., 2017).

We focus on summer when ozone pollution in China is most severe and when OMI has the strongest sensitivity (Zhang et al., 2010). Since 2009, certain cross-track OMI observations have degraded because of the so-called row anomaly (Kroon et al., 2011; Huang et al., 2017, 2018). We only use pixels that (1) pass the reported quality checks, (2) have a cloud fraction less than 0.3, and (3) have a solar zenith angle less than 60°. We exclude outliers with over 35 Dobson Units (DU) at 850-400 hPa (>99th percentile in eastern China) and exclude July 2011 when the retrievals are anomalously high.

The DOFS below 400 hPa over eastern China are in the range 0.3-0.6 (Figure 1a). The DOFS are generally higher in the south than in the north due to higher solar elevation in the south, and higher over China than in background air at the same latitude due to higher ozone abundances. We use DOFS > 0.3 in Figure 1a as criterion for further analysis; this excludes northern and western China. Although 0.3 is a relatively low DOFS threshold, the prior estimate is uniform other than a fixed latitudinal gradient in background ozone. To remove this gradient and also any long-term uniform drift in the data, we subtract the monthly mean Pacific background (150°E-150°W) for the corresponding latitude and month. The residual defines an OMI enhancement over China that we use for further analysis. This subtraction requires that we use a common pressure range for the OMI observations over China and the Pacific, but the OMI retrievals have variable pressure ranges depending on the local tropopause and surface pressures (Liu et al., 2010). The three lowest layers in the retrieval (L24-L22) have pressure ranges at sea level of approximately 1000-700 hPa, 700-500 hPa, and 500-350 hPa, and all contain some information on boundary layer ozone (Figure S1). Here we choose the pressure range 850-400 hPa to define the OMI enhancement relative to the Pacific background, and compute OMI columns for that pressure range by weighting the local L24-22 retrievals. The 850 hPa bottom pressure allows for topography.

To evaluate the ability of the OMI ozone enhancements to detect surface pollution, we use surface ozone measurements from the MEE network available for 2013-2017 (http://datacenter.mep.gov.cn/index). We select the summer (JJA) data at 12-15 local time (LT), corresponding to the OMI overpass. The network had 450 sites in 2013 and 1500 sites as of 2017, most located in large cities. We also use 2005-2016 summertime ozonesonde data for Hong Kong obtained from the World Ozone

© Author(s) 2018. CC BY 4.0 License.

and Ultraviolet Radiation Data Center (WOUDC) (http://woudc.org/), of which 57 days are coincident with OMI retrievals. The ozonesondes are launched at 13 LT. Data are often missing below 950 hPa and therefore we use data only above that level.

3 Summertime observations of ozone from the surface network, ozone sonde and OMI instrument

Figure 1b shows the mean midday (12-15 local time or LT) surface ozone for the summers of 2013-2017 as measured by the MEE network. Concentrations exceed 70 ppb over most of the North China Plain with particularly high values in the Beijing-Tianjin-Hebei (BTH) megacity cluster. Values are also high in the Yangtze River Delta (YRD), Pearl River Delta (PRD), Sichuan Basin (SCB), and the city of Wuhan in central China. High values extend to the region west of the North China Plain, which is less densely populated but has elevated terrain.

OMI mean ozone abundances at 850-400 hPa for the summers of 2013-2017 are shown in Figure 1c. Values are partial column concentrations in Dobson units (1 DU = 2.69×10^{16} molecules cm^{-2}). After subtracting the North Pacific background for the corresponding latitude in month, we obtain the OMI ozone enhancements shown in Figure 1d. There is strong spatial correlation (R = 0.73) between the OMI ozone enhancements and the MEE surface network. This demonstrates that OMI can successfully observe the mean spatial distribution of surface ozone over polluted regions. Critical to this success is the removal of the latitude-dependent Pacific background and the restriction to the domain with DOFS > 0.3. Figure 1e shows the corresponding scatterplot and the ordinary-least-squares (OLS) regression relating the OMI enhancement $\Delta\Omega$ to the 12-15 LT surface concentration [O_3] (the slope is 0.11 DU/ppb). From there one can estimate surface ozone (ppb) on the basis of the observed OMI enhancement (DU) as

$$[O_3] = 8.9\ \Delta\Omega + 15.8 \pm 10.7 \quad (1)$$

where the error standard deviation (precision) of 10.7 ppb is inferred from the scatterplot. With such a precision, OMI can provide useful information on surface ozone levels in polluted regions.

Capturing the day-to-day variability of surface ozone leading to high-ozone pollution episodes is far more challenging because of noise in individual retrievals. Figure 1f shows the OMI vs. MEE temporal correlation for the daily data. Correlation coefficients are consistently positive and statistically significant, but relatively weak. They are higher in South China (R = 0.3-0.6) than in North China (R = 0.1-0.3), reflecting the pattern of OMI information content (DOFS) in Figure 1a. This implies that OMI can provide statistical rather than deterministic temporal information on ozone pollution episodes, and we describe our statistical approach further down.

We examine in more detail the sensitivity of OMI to boundary layer ozone and its day-to-day variability versus the free troposphere by comparing to summertime 2005-2016 Hong Kong ozonesonde data. Figure 2a shows the measured

© Author(s) 2018. CC BY 4.0 License.

ozonesonde profiles (in ppb) mapped on a 100 hPa grid and selecting only the days when concurrent OMI retrievals are available (n = 57). The boundary layer ozone (950-850 hPa) in the ozonesonde data has large day-to-day variability, ranging from 20 to 120 ppb with a mean of 47 ppb. The variability in the free troposphere is much less.

Figure 2b shows the ozonesonde data smoothed by the OMI averaging kernel sensitivities for the corresponding retrievals. The retrievals over Hong Kong have a mean DOFS of 0.46 below 400 hPa. We see from Figure 2c that the OMI information is weighted toward the free troposphere but there is sensitivity in the boundary layer. The L23 ozone smoothed from the ozonesonde data in Figure 2b has a correlation coefficient of 0.75 with the 950-850 hPa ozone in the original data.

Figure 2d shows the OMI ozone retrievals coincident with the ozonesondes. We see that there is an overall good match with the sonde data smoothed by the averaging kernels. But we are most interested here in the ability of the OMI retrievals to detect the boundary layer (950-850 hPa) variability in the original ozonesonde data, before applying the averaging kernels. The temporal correlation coefficients of the 950-850 hPa ozonesonde data with the OMI retrievals at different levels are given in Figure 2d. The correlation coefficient with L23 OMI ozone is 0.51 (p<0.05), and the correlation coefficient with the 850-400 hPa OMI ozone constructed by weighting the L24-L23-L22 retrievals is 0.50. Figure 2e shows a scatterplot of the latter. We see that high-ozone episodes in the 950-850 hPa sonde data are systematically associated with high OMI values, though the converse does not always hold. For the 8 boundary layer episode days (> 82 ppb), the average OMI 850-400 hPa ozone is 23.7±3.1 DU, significantly higher than for the non-episode days (18.2±4.1 DU). The Hong Kong ozonesonde data thus demonstrate the potential of OMI to quantify the frequency of high-ozone episodes in the boundary layer even if it may not be reliable for individual events.

4 2005-2017 changes of ozone air quality in China as inferred from OMI

Figure 3 (top panel) further shows the relationship of daily MEE surface ozone concentrations with OMI enhancements when averaged spatially over each of the five megacity clusters identified in Figure 1. Consistent with the distribution of DOFS (Figure 1a), the correlations are higher in PRD, SCB, and Wuhan (0.42-0.53, p<0.05) than in YRD and BTH (0.27-0.35, p<0.05). The correlations indicate some capability for OMI to predict ozone daily variability on a statistical basis. The reduced axis regression (RMA) slopes are consistent across the five regions and average 0.15 DU/ppb. We define an ozone episode day by afternoon concentrations exceeding 82 ppb, corresponding to the Chinese air quality standard threshold. The bottom panel of Figure 3 compares the OMI ozone enhancements between episode and non-episode days as measured by the surface network. OMI is significantly higher (p<0.05) on episode days for all five regions.

Following on this statistical perspective, we construct a point process (PP) model from extreme value theory (Cole, 2001) to estimate the likelihood of surface ozone exceeding a high-ozone threshold u (here u = 82 ppb at 12-15 LT) at a given site i and day t given the observed OMI ozone enhancement $x_{i,t}$ for that day. The model describes the high tail of the ozone probability density function (pdf) as a Poisson process limit, conditioned on the local OMI observation. Such a model has

Atmos. Chem. Phys. Discuss., https://doi.org/10.5194/acp-2018-1246
Manuscript under review for journal Atmos. Chem. Phys.
Discussion started: 10 December 2018
© Author(s) 2018. CC BY 4.0 License.

Atmospheric Chemistry and Physics Discussions

been used previously to relate the probability of extreme air pollution conditions to meteorological predictor variables (Rieder et al., 2013; Shen et al., 2016, 2017) but here we use the OMI enhancement as predictor variable. We fit the model to all daily concurrent observations of surface ozone and OMI ozone enhancements for the ensemble of eastern China sites in Figure 1 (148,220 observations for summers 2013-2017). The probability of exceeding the threshold at a site *i* should depend not only on $x_{i,t}$ but also on its time-averaged value $\overline{x}_i$, because a high value of $\overline{x}_i$ means that a higher $x_{i,t}$ is less anomalous and more likely to represent an actual ozone exceedance than for a site with low $\overline{x}_i$. Thus the model has two predictor variables, $x_{i,t}$ and $\overline{x}_i$.

Details of the PP model can be found in Cole (2001). The model fits three parameters that control the shift, spread and shape of the high-tail pdf. The fit minimizes a cost function *L* given by

$$L = \prod_{i=1}^{m} L_i(\mu_i, \sigma_i, \xi) \tag{2}$$

with

$$L_i(\mu_i, \sigma_i, \xi) = exp\{-\frac{1}{n_a}\sum_{t=1}^{n}[1+\frac{\xi(u-\mu_i)}{\sigma_{i,t}}]^{-1/\xi}\}\prod_{t=1}^{n}\{\frac{1}{\sigma_{i,t}}[1+\frac{\xi(y_{i,t}-\mu_i)}{\sigma_{i,t}}]^{-1/\xi-1}\}^{I[y_{i,t}>u]} \tag{3}$$

$$\mu_i = \alpha_0 + \alpha_1\overline{x}_i \tag{4}$$

$$\overline{x}_i = \frac{1}{n}\sum_{t=1}^{n} x_{i,t} \tag{5}$$

$$\sigma_{i,t} = \exp(\beta_0 + \beta_1 x_{i,t}) \tag{6}$$

Here $L_i(\mu_i, \sigma_i, \xi)$ is the cost function for site *i* and *L* is for the total cost function for all *m* sites, $y_{i,t}$ is the daily 12-15 LT MEE surface ozone from each individual site *i* on day *t*, n_a =92 is the number of days in summer, μ_i is the location parameter for site *i* conditioned on the 2013-2017 summertime mean OMI enhancements $\overline{x}_i$, $\sigma_{i,t}$ is the scale parameter conditioned on the local OMI ozone enhancements $x_{i,t}$, ξ is the shape factor, and $I[y_{i,t}>u]$ is one if observed ozone is above the threshold and zero otherwise. Minimization of the cost function optimizes the values of the parameters α_0, α_1, β_0, β_1, and ξ given the 148,220 ($x_{i,t}$, $y_{i,t}$) data pairs for eastern China. The resulting values are α_0 = 110 ppb, α_1 = 4.5, β_0 = 2.7 ppb, β_1 = -0.019, ξ = -0.13. The probability of daily ozone exceeding the threshold *u* is then calculated as

Atmos. Chem. Phys. Discuss., https://doi.org/10.5194/acp-2018-1246
Manuscript under review for journal Atmos. Chem. Phys.
Discussion started: 10 December 2018
© Author(s) 2018. CC BY 4.0 License.

Atmospheric Chemistry and Physics Discussions

$$p(y_{i,t} \geq u \mid x_{i,t}) = \frac{1}{n_a}[1+\xi(\frac{u-\mu_i}{\sigma_{i,t}})]^{-1/\xi} \quad (7)$$

The model is optimized using the *extRemes* package in R (Gilleland and Katz, 2011). We performed a 10-fold cross validation of the model, in which we partitioned the sites into 10 equal subsets and repeatedly used one subset as testing data and the rest as training data. The results show that the predicted fraction of ozone episodes resemble that of observed, with a spatial correlation of 0.68 (Figure 4a-b). 82 ppb corresponds to the 80th percentile of the data, which is a relatively low threshold for application of extreme value theory. However, we find that the resulting model can also accurately estimate the probability of exceedance above higher thresholds (Figure 4c), which confirms the property of threshold invariance of an extreme value model (Cole, 2001). We also tested the model with uniform location or scale factors, neither of which can reproduce the observed spatial distribution of ozone episodes.

We can use the long-term OMI ozone record for 2005-2017 to infer trends in surface ozone over China. Figure 5 shows the changes between 2013-2017 and 2005-2009 in mean summer afternoon ozone concentrations and in the number of high-ozone episode days per summer. The changes in mean summer afternoon ozone concentrations are obtained from the difference in the mean OMI enhancements at 850-400 hPa and applying equation (1). The changes in the number of high-ozone episode days are obtained by applying the probability of exceeding 82 ppb (equation 7) to each pair of 5 years of OMI data. When averaged across eastern China, the mean summer afternoon ozone concentrations have increased by 5.4 ppb (0.67 ppb a^{-1}) and the number of ozone episodes (> 82 ppb) has increased by 2.8 days (0.34 days a^{-1}) over the 8-year period.

We find worsening conditions for ozone pollution all across eastern China and particularly in BTH, Shandong Province, and downwind in Liaoning Province. The mean summertime afternoon ozone in BTH increases by 1.0±0.5 ppb a^{-1} over the duration of the OMI record (Figure 5a), which is consistent with the 2003-2015 observed trend of 1.1 ppb a^{-1} at the Shangdianzi site (100 km northeast of Beijing) (Ma et al., 2016). The frequency of ozone episodes increases at a rate of 0.84±0.41 days a^{-1} in BTH, much higher than in southern China (Figure 5b).

One might expect nonlinearity in the ozone trend over the 2005-2017 period; for example, NO_x emissions in China peaked in 2011 and have been decreasing since (Zheng et al., 2018). We tried to diagnose a finer temporal structure in the OMI trend but were unsuccessful because of noise, as illustrated in Figure S2 with the annual time series of high-ozone episodes for BTH. The interannual variability amplifies after 2009, which may be related to degradation of OMI data quality due to the row anomaly (see Data and Methods section).

Atmos. Chem. Phys. Discuss., https://doi.org/10.5194/acp-2018-1246
Manuscript under review for journal Atmos. Chem. Phys.
Discussion started: 10 December 2018
© Author(s) 2018. CC BY 4.0 License.

Atmospheric Chemistry and Physics Discussions

5 Discussion and conclusion

The GEMS (Geostationary Environment Monitoring Spectrometer) satellite instrument is expected to launch in 2019 and will observe East Asia with a spectral range, resolution, and accuracy similar to OMI (Bak et al., 2013). GEMS will have much higher data density than OMI including finer pixels (7×8 km^2 vs. 13×24 km^2) and more frequent return time (hourly vs. daily). Our results suggest that the continuous measurements from GEMS should be of considerable value for monitoring ozone pollution episodes in the region. The TEMPO (Tropospheric Emissions: Monitoring of Pollution) geostationary satellite instrument to be launched around 2020 over North America will have a spectral range extending to the visible Chappuis bands where ozone detection sensitivity remains high down to the surface (Zoogman et al., 2011, 2017). This will allow for improved observations of surface ozone, particularly where concentrations are not as high as they are presently in China.

In summary, we have used the dense 2013-2017 ozone network data from the China Ministry of Ecology and Environment (MEE) to evaluate the ability of the OMI satellite instrument to map the distribution of surface ozone pollution in China and detect high-ozone episodes on a daily basis. Although the OMI retrieval for tropospheric ozone is weighted toward the middle troposphere, it can also detect elevated levels in the boundary layer as shown by analysis of Hong Kong ozonesonde data. We removed the monthly mean latitude-dependent Pacific background to define OMI enhancements over China. From there we found that the OMI observations can quantify mean summer afternoon surface concentrations of ozone over China with a precision of 10.7 ppb, and can reproduce the observed spatial variability of these concentrations (R = 0.73). Day-to-day correlation coefficients between OMI enhancements and the surface ozone network data are in the range 0.3-0.6 in southern China and 0.1-0.3 in northern China, implying that the frequency of high-ozone episodes can be detected from OMI on a statistical basis. OMI enhancements are significantly higher on observed surface episode days (>82 ppb, corresponding to the Chinese air quality standard threshold) relative to non-episode days. We used a point process model from extreme value theory to successfully infer the probability of surface ozone exceeding 82 ppb or higher thresholds on the basis of the daily observed OMI ozone enhancements. The long-term OMI record shows a general increase in mean summertime surface ozone and in the frequency of high-ozone episodes across eastern China for the 2005-2017 period. Our method for inferring surface ozone pollution and the frequency of high-ozone episodes from the OMI data can be applied to countries outside China where surface observations are not available.

© Author(s) 2018. CC BY 4.0 License.

Author contribution

L. Shen and D. Jacob designed the experiments and L. Shen carried them out. X. Liu and G. Huang provided the satellite data. K. Li and H. Liao provided the surface observations. L. Shen and D. Jacob prepared the manuscript with contributions from all co-authors.

Acknowledgments

This work was funded by the NASA Earth Science Division, by the Harvard Global Institute (HGI), and by the Joint Laboratory for Air Quality and Climate (JLAQC) between Harvard and the Nanjing University for Information Sciences and Technology (NUIST).

Reference

Bell, M.L., McDermott, A., Zeger, S.L., Samet, J.M. and Dominici, F.: Ozone and short-term mortality in 95 US urban communities, 1987-2000, JAMA, 292(19), 2372-2378, 2004.

Bak, J., Kim, J. H., Liu, X., Chance, K., and Kim, J.: Evaluation of ozone profile and tropospheric ozone retrievals from GEMS and OMI spectra, Atmos. Meas. Tech., 6, 239-249, http://sci-hub.tw/10.5194/amt-6-239-2013, 2013.

Coles, S. G.: An Introduction to Statistical Modeling of Extreme Values, Springer, New York, 2001.

Eremenko, M., Dufour, G., Foret, G., Keim, C., Orphal, J., Beekmann, M., Bergametti, G., and Flaud, J.-M.: Tropospheric ozone distributions over Europe during the heat wave in July 2007 observed from infrared nadir spectra recorded by IASI, Geophys. Res. Lett., 35, L18805, doi:10.1029/2008GL034803, 2008.

Fishman, J., Vukovich, F. M., Cahoon, D. R., and Shipham, M. C.: The characterization of an air pollution episode using satellite total ozone measurements, J. Clim. Appl. Meteorol., 26, 1638– 1654, 1987.

Gao W, et al.: Long-term trend of O3 in a mega City (Shanghai), China: Characteristics, causes, and interactions with precursors, Sci. Total. Environ., 603, 425-433, 2017.

Gilleland, E., Katz, R. W.: New software to analyze how extremes change over time, Eos Trans. AGU, 92(2), 13–14, doi:10.1029/2011EO020001, 2011.

Hayashida, S., Urita, N., Noguchi, K., Liu, X., and Chance, K.: Spatiotemporal Variation in Tropospheric Column Ozone over East Asia Observed by GOME and Ozonesondes, Sola, 4, 117–120, 2008.

Hu, L., Jacob, D. J., Liu, X., Zhang, Y., Zhang, L., and Kim, P. S.: Global budget of tropospheric ozone: evaluating recent model advances with satellite (OMI), aircraft (IAGOS), and ozonesonde observations, Atmos. Environ., 1–36, 2017.

© Author(s) 2018. CC BY 4.0 License.

Huang, G., Liu, X., Chance, K., Yang, K., Bhartia, P. K., Cai, Z., Allaart, M., Ancellet, G., Calpini, B., Coetzee, G. J. R., Cuevas-Agulló, E., Cupeiro, M., De Backer, H., Dubey, M. K., Fuelberg, H. E., Fujiwara, M., Godin-Beekmann, S., Hall, T. J., Johnson, B., Joseph, E., Kivi, R., Kois, B., Komala, N., König-Langlo, G., Laneve, G., Leblanc, T., Marchand, M., Minschwaner, K. R., Morris, G., Newchurch, M. J., Ogino, S.-Y., Ohkawara, N., Piters, A. J. M., Posny, F., Querel, R., Scheele, R., Schmidlin, F. J., Schnell, R. C., Schrems, O., Selkirk, H., Shiotani, M., Skrivánková, P., Stübi, R., Taha, G., Tarasick, D. W., Thompson, A. M., Thouret, V., Tully, M. B., Van Malderen, R., Vömel, H., von der Gathen, P., Witte, J. C., and Yela, M.: Validation of 10-year SAO OMI Ozone Profile (PROFOZ) product using ozonesonde observations, Atmos. Meas. Tech., 10, 2455-2475, http://sci-hub.tw/10.5194/amt-10-2455-2017, 2017.

Huang, G., Liu, X., Chance, K., Yang, K., and Cai, Z.: Validation of 10-year SAO OMI ozone profile (PROFOZ) product using Aura MLS measurements, Atmos. Meas. Tech., 11, 17-32, http://sci-hub.tw/10.5194/amt-11-17-2018, 2018.

Kar, J., Fishman, J., Creilson, J. K., Richter, A., Ziemke, J., and Chandra, S.: Are there urban signatures in the tropospheric ozone column products derived from satellite measurements?, Atmos. Chem. Phys., 10, 5213-5222, http://sci-hub.tw/10.5194/acp-10-5213-2010, 2010.

Kim, P. S., Jacob, D. J., Liu, X., Warner, J. X., Yang, K., Chance, K., Thouret, V., and Nedelec, P.: Global ozone–CO correlations from OMI and AIRS: constraints on tropospheric ozone sources, Atmos. Chem. Phys., 13, 9321-9335, http://sci-hub.tw/10.5194/acp-13-9321-2013, 2013.

Kroon, M., de Haan, J. F., Veefkind, J. P., Froidevaux, L., Wang, R., Kivi, R., and Hakkarainen, J. J.: Validation of operational ozone profiles from the Ozone Monitoring Instrument, J. Geophys. Res., 116, D18305, doi:10.1029/2010JD015100, 2011.

Levelt, P. F., Van den Oord, G. H. J., Dobber, M. R., Malkki, A., Visser, H., de Vries, J., Stammes, P., Lundell, J. O. V., and Saari, H.: The Ozone Monitoring Instrument, IEEE T. Geosci. Remote, 44, 1093–1101, 2006.

Liu, X., Bhartia, P. K., Chance, K., Spurr, R. J. D., and Kurosu, T. P.: Ozone profile retrievals from the Ozone Monitoring Instrument, Atmos. Chem. Phys., 10, 2521-2537, http://sci-hub.tw/10.5194/acp-10-2521-2010, 2010.

Ma, Z., Xu, J., Quan, W., Zhang, Z., Lin, W., and Xu, X.: Significant increase of surface ozone at a rural site, north of eastern China, Atmos. Chem. Phys., 16, 3969-3977, http://sci-hub.tw/10.5194/acp-16-3969-2016, 2016.

McPeters, R. D., Labow, G. J., and Logan, J. A.: Ozone climatological profiles for satellite retrieval algorithms, J. Geophys. Res., 112, D05308, doi:10.1029/2005JD006823, 2007.

Rieder, H. E., Fiore, A. M., Polvani, L. M., Lamarque, J. F., and Fang, Y.: Changes in the frequency and return level of high ozone pollution events over the eastern United States following emission controls, Environ. Res. Lett., 8, 014012, doi:10.1088/1748- 9326/8/1/014012, 2013.

Shen, L., Mickley, L. J., Gilleland E. : Impact of increasing heat waveson U.S. ozone episodes in the 2050s: Results from a multimodel analysisusing extreme value theory, Geophys.Res. Lett.,43, 4017–4025, doi:10.1002/2016GL068432, 2016

© Author(s) 2018. CC BY 4.0 License.

Shen, L., Mickley, L. J., Leibensperger, E.M., Li, M.: Strong dependenceof U.S. summertime air quality on thedecadal variability of Atlantic sea surface temperatures, Geophys. Res. Lett., 44, 12,527–12,535. https://doi.org/10.1002/2017GL075905, 2017

Shim, C., Li, Q., Luo, M., Kulawik, S., Worden, H., Worden, J., Eldering, A., Diskin, G., Sachse, G., Weinheimer, A., Knapp, D., Montzca, D., Campos, T.: Satellite observations of Mexico City pollution outflow from the Tropospheric Emissions Spectrometer (TES), Atmos. Environ., 43(8), 1540–1547, 2009.

Sun, L., Xue, L., Wang, T., Gao, J., Ding, A., Cooper, O. R., Lin, M., Xu, P., Wang, Z., Wang, X., Wen, L., Zhu, Y., Chen, T., Yang, L., Wang, Y., Chen, J., and Wang, W.: Significant increase of summertime ozone at Mount Tai in Central Eastern China, Atmos. Chem. Phys., 16, 10637-10650, http://sci-hub.tw/10.5194/acp-16-10637-2016, 2016.

Wang, T., Xue, L. K., Brimblecombe, P., Lam, Y. F., Li, L., and Zhang, L.: Ozone pollution in China: A review of concentrations, meteorological influences, chemical precursors, and effects, Sci. Total Environ., 575, 1582–1596, 2017.

Zheng, B., Tong, D., Li, M., Liu, F., Hong, C., Geng, G., Li, H., Li, X., Peng, L., Qi, J., Yan, L., Zhang, Y., Zhao, H., Zheng, Y., He, K., and Zhang, Q.: Trends in China's anthropogenic emissions since 2010 as the consequence of clean air actions, Atmos. Chem. Phys., 18, 14095-14111, http://sci-hub.tw/10.5194/acp-18-14095-2018, 2018.

Zoogman, P., Jacob, D. J., Chance, K., Zhang, L., Sager, P. L., Fiore, A. M., Eldering, A., Liu, X., Natraj, V., and Kulawik, S. S.: Ozone air quality measurement requirements for a geostationary satellite mission, Atmos. Environ., 45, 7143–7150, 2011.

Zoogman, P., Liu, X., Suleiman, R. M., Pennington, W. F., Flittner, D. E., Al, Saadi, J. A., et al.: Tropospheric emissions: Monitoring of pollution (TEMPO), J. Quant. Spectrosc. Radiat. Transf., 186, 17–39. https://doi.org/10.1016/j.jqsrt.2016.05.008, 2017.

Ziemke, J. R., Chandra, S., Labow, G. J., Bhartia, P. K., Froidevaux, L., and Witte, J. C.: A global climatology of tropospheric and stratospheric ozone derived from Aura OMI and MLS measurements, Atmos. Chem. Phys., 11, 9237-9251, http://sci-hub.tw/10.5194/acp-11-9237-2011, 2011.

Zhang, L., Jacob, D. J., Liu, X., Logan, J. A., Chance, K., Eldering, A., and Bojkov, B. R.: Intercomparison methods for satellite measurements of atmospheric composition: application to tropospheric ozone from TES and OMI, Atmos. Chem. Phys., 10, 4725-4739, http://sci-hub.tw/10.5194/acp-10-4725-2010, 2010.

Atmos. Chem. Phys. Discuss., https://doi.org/10.5194/acp-2018-1246
Manuscript under review for journal Atmos. Chem. Phys.
Discussion started: 10 December 2018
© Author(s) 2018. CC BY 4.0 License.

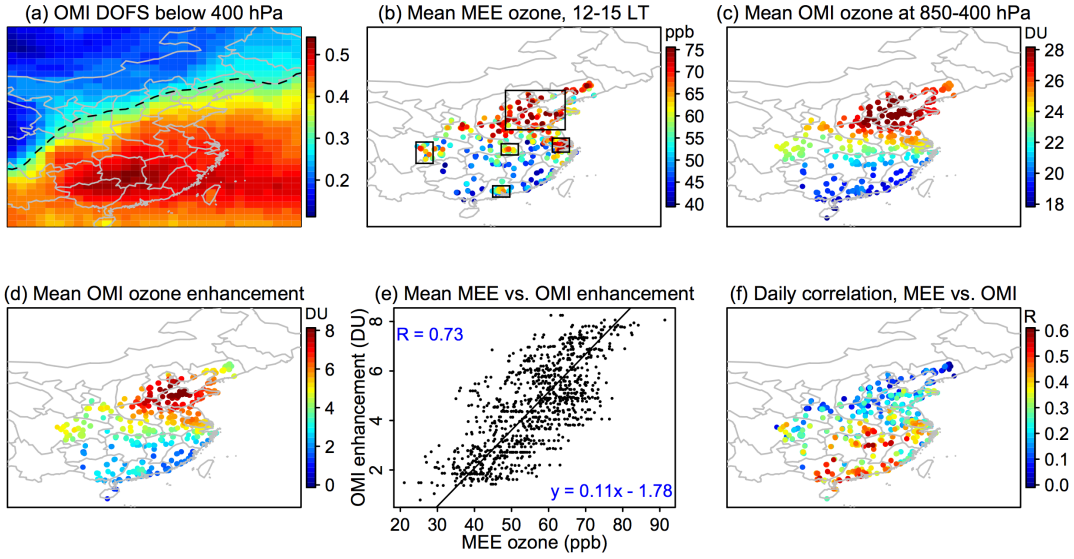

Figure 1. Summertime observations of ozone over China (JJA 2013-2017) from the MEE surface network and the OMI satellite instrument. (a) Mean degrees of freedom for signal (DOFS) of OMI ozone retrievals below 400 hPa. We limit our attention to the China domain with DOFS > 0.3 (dashed line) and to sites with at least 100 concurrent surface and OMI observations for the 2013-2017 period. (b) Mean midday (12-15 local time) ozone concentrations from the MEE surface network. Rectangles identify high-ozone regions discussed in the text including Beijing-Tianjing-Hebei (BTH, 114°-121°E, 34-41°E), Yangtze River Delta (YRD, 119.5°-121.5°E, 30-32.5°E), Pearl River Delta (PRD, 112.5°-114.5°E, 22-24°E), Sichuan Basin (SCB, 103.5°-105.5°E, 28-31.5°E), and Wuhan (113.5°-115.5°E, 29.5-31.5°E). (c) Mean OMI partial columns at 850-400 hPa. (d) Mean OMI ozone enhancements at 850-400 hPa after subtraction of the latitude-dependent mean background in that same pressure range over the Pacific (150°E-150°W). (e) Relationship of mean MEE ozone and the OMI ozone enhancement at 850-400 hPa. The correlation coefficient and the fitted ordinary linear regression (OLS) equation are shown inset. (f) Temporal correlation coefficients (R) of daily MEE surface ozone with OMI, measuring the ability of OMI to capture the day-to-day variability of surface ozone.

Atmos. Chem. Phys. Discuss., https://doi.org/10.5194/acp-2018-1246
Manuscript under review for journal Atmos. Chem. Phys.
Discussion started: 10 December 2018
© Author(s) 2018. CC BY 4.0 License.

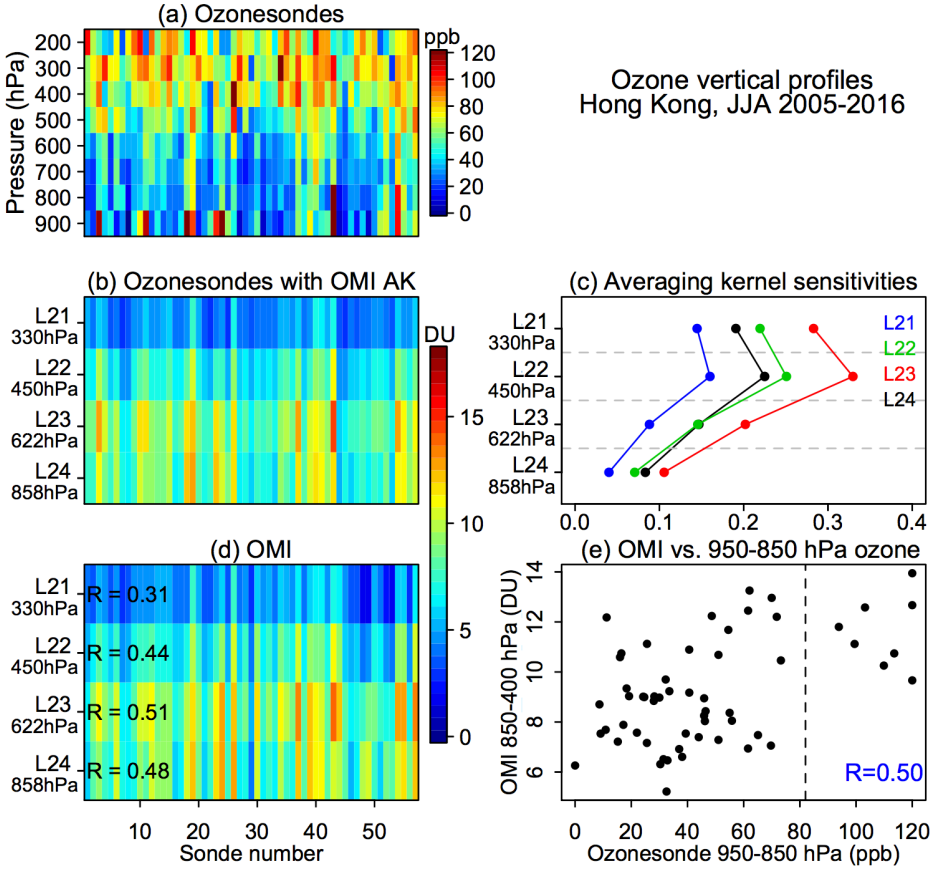

Figure 2. Ozone vertical profiles over Hong Kong in summer (JJA) 2015-2016. (a) Ozonesonde data coincident with OMI observations (*n*=57), averaged over a 100 hPa grid and arranged in chronological order (b) The same ozonesonde data but smoothed by the OMI averaging kernels. Mean pressures for each OMI retrieval level are indicated. (c) Mean averaging kernel sensitivities for each OMI retrieval level, as described by the rows of the averaging kernel matrix; values are shown for August 2015 but are similar in other summer months and years. The dashed lines are boundaries between retrieval levels. (d) OMI ozone observations coincident with the ozonesondes. The correlations of unsmoothed 950-850 hPa ozonesonde data with the OMI retrievals for different levels are shown inset. (e) Relationship of unsmoothed 950-850 hPa ozonesonde data and OMI 850-400 hPa ozone. The correlation is shown inset. The dashed line corresponds to the Chinese ozone air quality standard (82 ppb).

Atmos. Chem. Phys. Discuss., https://doi.org/10.5194/acp-2018-1246
Manuscript under review for journal Atmos. Chem. Phys.
Discussion started: 10 December 2018
© Author(s) 2018. CC BY 4.0 License.

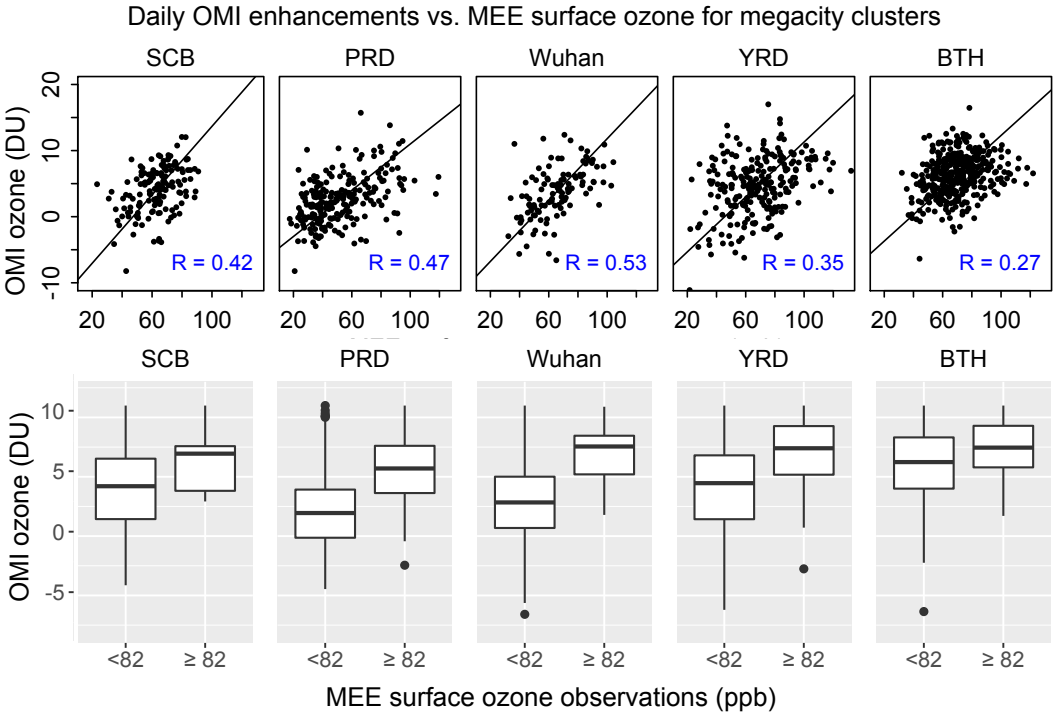

Figure 3. Ability of daily OMI observations to detect high-ozone episodes in the five megacity clusters of Figure 1. Daily surface afternoon (12-15 local time) observations from the MEE network in summer (JJA) 2013-2017 averaged over the megacity clusters are compared to the corresponding OMI enhancements relative to the Pacific background. The top panels show the correlations in the daily data, with correlation coefficients inset. Reduced-major-axis (RMA) linear regression lines are also shown. The bottom panels show the distributions of OMI enhancements for episode (> 82 ppbv) and non-episode (< 82 ppbv) days. The top and bottom of each box are the 25th and 75th percentiles, the centerline is the median, the vertical bars are the 2th and 98th percentiles, and the dots are outliers.

Atmos. Chem. Phys. Discuss., https://doi.org/10.5194/acp-2018-1246
Manuscript under review for journal Atmos. Chem. Phys.
Discussion started: 10 December 2018
© Author(s) 2018. CC BY 4.0 License.

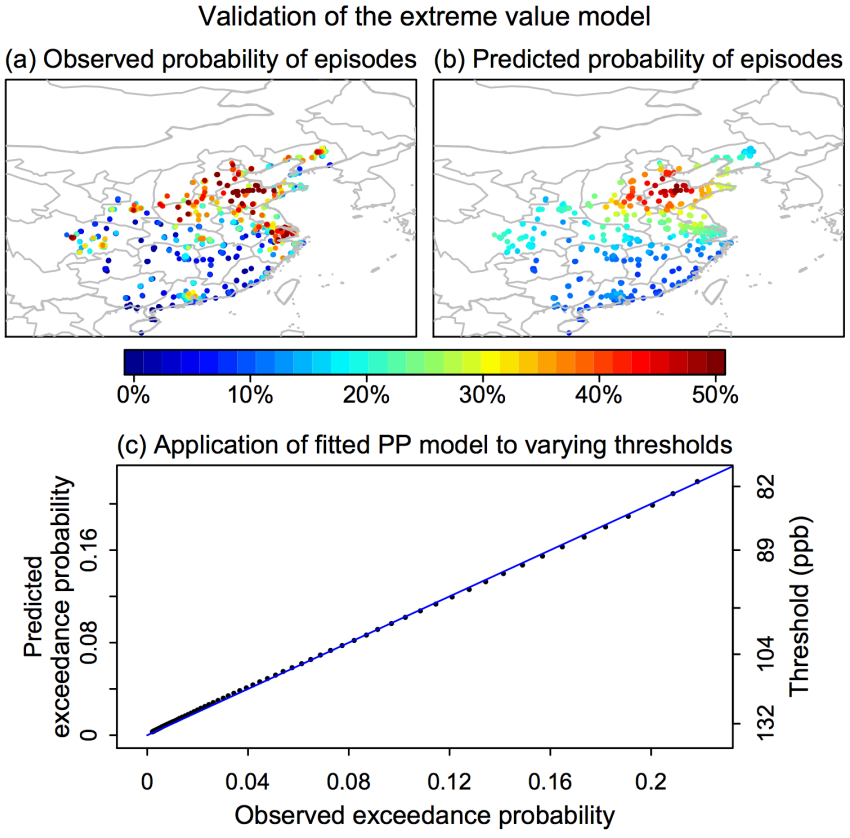

Figure 4. Validation of the extreme value model. (a) Observed probability of ozone episode days (> 82 ppb). (b) Predicted probability of ozone episode days, calculated by applying the probability of exceeding 82 ppb (equation 7). (c) Predicted probability of exceedance above a higher threshold (> 82 ppb) using Equation 7. The blue line denotes the 1:1 reference line.

Atmos. Chem. Phys. Discuss., https://doi.org/10.5194/acp-2018-1246
Manuscript under review for journal Atmos. Chem. Phys.
Discussion started: 10 December 2018
© Author(s) 2018. CC BY 4.0 License.

Atmospheric Chemistry and Physics Discussions

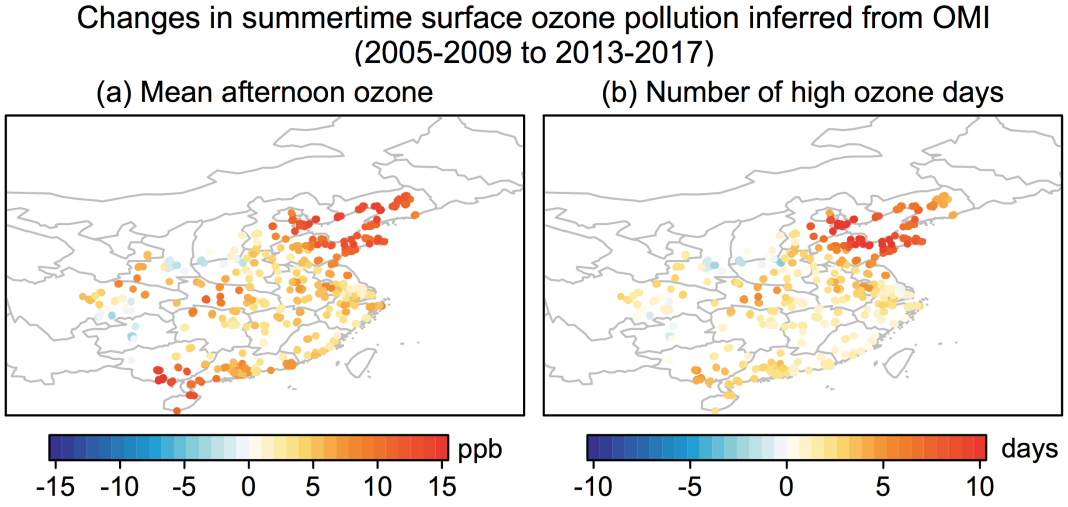

Figure 5. Changes in surface ozone pollution in China between 2005-2009 and 2013-2017 as inferred from OMI observations. (a) Change in mean summer afternoon concentrations, obtained from the difference in the mean OMI enhancements at 850-400 hPa and applying equation (1). (b) Change in the number of ozone episodes (> 82 ppb) per summer, calculated by applying the probability of exceeding 82 ppb (equation 7) to the daily OMI enhancements.